Relaxation processes at the glass transition in polyamide 11: From rigidity to viscoelasticity

Peter Frübing,[a] Alexander Kremmer, and Reimund Gerhard-Multhaupt
Department of Physics, University of Potsdam, Am Neuen Palais 10, D-14469 Potsdam, Germany

Anna Spanoudaki and Polycarpos Pissis
Department of Physics, National Technical University of Athens, Zografou Campus, GR-15773 Athens, Greece

(Received 15 March 2006; accepted 11 September 2006; published online 1 December 2006)

Relaxation processes associated with the glass transition in nonferroelectric and ferroelectric polyamide (PA) 11 are investigated by means of differential scanning calorimetry, dynamic mechanical analysis, and dielectric relaxation spectroscopy (DRS) in order to obtain information about the molecular mobility within the amorphous phase. In particular, the effects of melt quenching, cold drawing, and annealing just below the melting region are studied with respect to potential possibilities and limitations for improving the piezoelectric and pyroelectric properties of PA 11. A relaxation map is obtained from DRS that shows especially the crossover region where the cooperative α relaxation and the local β relaxation merge into a single high-temperature process. No fundamental difference between quenched, cold-drawn, and annealed films is found, though in the cold-drawn (ferroelectric) film the α relaxation is suppressed and slowed down, but it is at least partly recovered by subsequent annealing. It is concluded that there exists an amorphous phase in all structures, even in the cold-drawn film. The amorphous phase can be more rigid or more viscoelastic depending on preparation. Cold drawing not only leads to crystallization in a ferroelectric form but also to higher rigidity of the remaining amorphous phase. Annealing just below the melting region after cold drawing causes a stronger phase separation between the crystalline phase and a more viscoelastic amorphous phase. © *2006 American Institute of Physics*. [DOI: 10.1063/1.2360266]

I. INTRODUCTION

Like the other odd-numbered polyamides, polyamide 11 (PA 11) is a ferroelectric polymer. The ferroelectricity is caused by the existence of a *doubly oriented hydrogen-bonded sheet structure*.[1] It forms a crystalline phase in which the aliphatic chains are aligned in parallel, while their amide-group dipoles are oriented perpendicular to the chain direction. Due to the odd number of carbon atoms per repeating unit, all –NH–CO– dipole moments have components that point in the same direction rather than alternating as in the even-numbered polyamides. The situation is analogous to the ferroelectric poly(vinylidene fluoride) (PVDF) or its copolymers with trifluoroethylene (PVDF-TrFE). However, even though PA 11 and PVDF have comparable coercive fields and remanent polarizations,[2] the room-temperature piezoelectric activity of PA 11 is significantly lower. It was not possible up to now to obtain significantly higher piezoelectric coefficients than about 4 pC/N at room temperature. This is related to the different glass-transition temperatures of PA 11 and PVDF which lie above (≈50 °C) and below (≈−30 °C) room temperatures, respectively. On the other hand, the piezoelectric activity of PA 11 shows a better thermal stability up to temperatures close to its melting range (170 °C) than PVDF.[3]

Parallel alignment of the polyamide chains is forced by stretching the PA-11 film uniaxially at room temperature (cold drawing). A stretching ratio of nearly 3:1 can be achieved. PA 11 is a semicrystalline polymer that crystallizes very fast in a nonpolar form. However, quenching from the melt can prevent the growth of large-sized crystallites, and thus makes cold drawing more effective. Therefore, ferroelectric PA-11 films are usually prepared by melting the powder in a hot press, quenching in ice water or liquid nitrogen, and subsequently cold drawing. Another way is extrusion onto a cooled steel roller and subsequent cold drawing in the extrusion direction. Finally, dipole orientation is achieved by electric poling above the coercive field. Annealing just below the melting region after poling is applied in order to stabilize the piezoelectric response. However, annealed PA-11 films do not show ferroelectric switching of the polarization.[4]

In 1990, Xenopoulus and Wunderlich[5] published a detailed calorimetric study on thermodynamic properties of aliphatic polyamides. They found that there exists a rigid amorphous phase (RAP) in all semicrystalline aliphatic polyamides, including PA 11. The existence of a third phase between the crystalline phase and the viscoelastic amorphous phase in several semicrystalline polymers has been extensively discussed during the last 20 years. Usually it is deduced from discrepancies in the fraction of mobile chain segments determined from dielectric relaxation strength and the

[a]Author to whom correspondence should be addressed. Electronic mail: fruebing@rz.uni-potsdam.de

amount of amorphous fraction determined by differential scanning calorimetry (DSC) or x-ray measurements.[6] The formation of the RAP manifests itself in DSC scans as a deficiency in the specific-heat step at the glass transtion and a negative contribution to the specific heat c_p between the glass transition and the melting region which is, however, often compensated by an increase of c_p due to conformational motion. In several polymers the RAP may even have a separate glass transition, but in polyamides (particularly PA 6, PA 12) only a broadening of the glass transition is observed.[7]

The RAP has been attributed with order-disorder interfaces at crystal surfaces or with interlamellar noncrystalline regions. However, the RAP does not represent a well-defined phase since the molecular mobility changes continuously between the crystal surface and the remaining meltlike regions.[8] The RAP is persistent above the glass transition of the viscoelastic amorphous phase, but it will be progressively mobilized with increasing temperature and therefore gradually lose its character as a separate phase.[9] Consequently, thermal treatment should be able to reduce or restore it to some extent.[10] In polyamides there is certainly an additional contribution to rigidity which comes from hydrogen bonding. Cross-linking via hydrogen bonds makes the whole amorphous phase more or less rigid and therefore blurs the phase boundaries.

It can be expected that amide-group dipoles within the RAP cannot be well oriented in an external electric field and therefore do not contribute to the polarization and the piezoelectric effect or do not give a thermally stable polarization. The question arises whether it is possible to overcome this limitation at least partly by optimizing the preparation process. To answer this question information about relaxation processes in PA 11 and their changes during the preparation steps of ferroelectric films are necessary.

In this study, DSC, dynamic mechanical analysis (DMA), and dielectric relaxation spectroscopy (DRS) in combination with thermally stimulated depolarization-current (TSDC) measurements are applied in order to study the effects of quenching, cold drawing, and annealing on thermal transitions and relaxation processes in PA 11. The aims are (1) to check previous results of dielectric measurements[11,12] about structural changes that result from quenching, cold drawing, and annealing with additional measurements (DSC and DMA) and (2) to conduct a more detailed dielectric-data analysis, particularly in the range of the α relaxation that is connected with the glass transition. A better insight into this relaxation process could help to identify possible contributions of amide-group dipoles in the amorphous phase to the electric polarization and thus to the piezo- and pyroelectric activities of PA 11.

II. SAMPLE PREPARATION AND EXPERIMENTAL PROCEDURES

For DSC and DMA measurements, extruded films of commercial grade (RILSAN® B, composition B ES HV O without additives) were used. They had been quenched on a massive steel roller at room temperature immediately after passing the nozzle. For DRS freestanding films were prepared from powder of commercial grade (composition T, Naturelle, B HV COS, grain size 120 μm). Two series of DRS measurements were performed. For the first series, the powder was melted between two stainless-steel plates in a hot press, then the melt was pressed at about 210 °C into a thin film (thickness on the order of 50 μm), and the plates with the film between them were subsequently quenched in ice water. For the second series, the powder was melted at 230 °C on a stainless-steel plate under nitrogen. Then the plate with the molten layer on it was quenched in ice water (film thickness about 500 μm). Uniaxial stretching was performed at room temperature (cold drawing) with a ratio of typically 2.5:1 to 2.8:1, using a Zwick 1445 materials-testing apparatus. Homogeneity of drawing was checked by means of a grid that had been painted onto the film.

DSC measurements were performed on a PerkinElmer Pyris Diamond DSC. The glass transition was investigated with the StepScan™ technique, whereas the melting region was measured in the standard DSC mode (heating rate 20 K/min). The StepScan™ technique is the time-domain variant of the temperature-modulated DSC. The approach applies a series of short heating intervals ΔT_{step} with a heating rate h and isothermal hold steps Δt_{iso} to cover the temperature range of interest (here $\Delta T_{\mathrm{step}}=2.0$ K, $h=20$ K/min, $\Delta t_{\mathrm{iso}}=60$ s). It allows for accurate specific-heat (c_p) measurements because it enables the separation of the thermodynamic c_p signal (reversible) from the kinetic response (irreversible) of the material. It is particularly advantageous if weak thermal transitions have to be measured.[13] Always, only the first heating run is considered. Selected films were annealed 30 min at 170 °C followed by cooling with 200 K/min to room temperature prior to the measurement.

DMA measurements were performed on a DMA 242C (Netzsch) at 10 Hz and at a constant amplitude of 20 μm in the temperature range from −50 to 160 °C under nitrogen atmosphere (sample area about 7×5 mm^2, sample thickness about 100 μm). Selected films were annealed for 60 min at 160 °C followed by cooling with 3 K/min to room temperature prior to the measurement.

DRS was performed from −20 to +120 °C and 0.3 Hz to 1 MHz (first series), or from +20 to +120 °C and from 10 Hz to 10 MHz as well as from +100 to +170 °C and from 1 MHz to 1 GHz (second series). The Novocontrol Alpha frequency-response analyzer for low-frequency (LF) measurements (below 10 MHz) and the Hewlett-Packard 4291B rf impedance/material analyzer for high-frequency (HF) measurements (above 1 MHz) were employed together with the Quatro cryosystem. The data were acquired as a function of frequency under nearly isothermal conditions ($\Delta T_{\mathrm{max}}=0.25$ K) in steps of 4 K (first series) or 2.5 K (second series). For LF measurements, aluminum electrodes (thickness about 50 nm, diameter of 10 or 8 mm) were evaporated on the samples. Then the films were mounted between two polished stainless-steel plates in the sample holder. For HF measurements, the nonevaporated film was mounted directly between circular gold-plated electrodes (diameter of 6 mm). All measurements were performed under dry nitrogen. The films of the second series were dried in the sample holder for 1 h at 20 °C under nitrogen prior to the

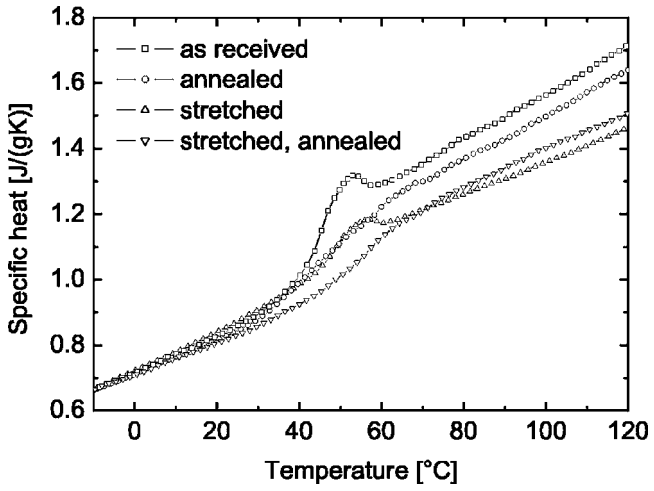

FIG. 1. Glass transitions of PA-11 films after different preparations as indicated.

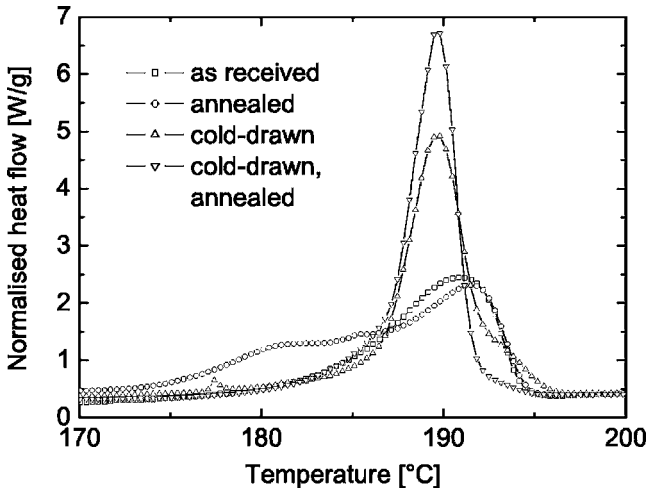

FIG. 2. Melting regions of PA-11 films after different preparations as indicated.

measurement. After the DRS measurement, the films were annealed for 30 min just below the melting region (at 170 °C) under nitrogen. Finally, the DRS measurement was repeated in order to study the effect of annealing.

For TSDC measurements, samples prepared in the same manner as for the first series of DRS were mounted between the plates of a capacitor and polarized under an electric field $E_p=1.0$ MV/m at the polarizing temperature T_p for $t_p=5$ min, a time much longer than the relaxation time at T_p, so that a maximum polarization was achieved. Then the sample was cooled down under field with a cooling rate of 10 K/min to a temperature T_0, and finally the field was removed and the sample reheated at a constant rate of 3 K/min. The discharge current was recorded as a function of temperature using a Keithley 617 electrometer. The measurements were performed under dry nitrogen. The temperature was controlled using the Quatro cryosystem and ranged between −140 and 80 °C. All samples were treated at 100 °C prior to the measurement in order to remove excess charges possibly accumulated during storage. The measurements were repeated for each sample with different polarization temperatures varying between 55 and 65 °C.

In the following chapter four types of films are compared: the as-received (extruded or melt-quenched) film, the annealed film, the cold-drawn film, and the cold drawn and then annealed film.

III. RESULTS AND DISCUSSION

A. Differential scanning calorimetry (DSC)

The glass transitions of extruded PA 11 films are presented in Fig. 1. All films show a glass transition, in particular, the cold-drawn film. The glass-transition temperatures T_g are around 50 °C. No significant shift of T_g can be observed after different preparations. However, the determination of T_g is uncertain because of the endothermal peaks which appear in the thermograms of the nonannealed films. They are a typical phenomenon that is observed on slowly cooled or annealed glasses.[14] For PA 11, these peaks have been attributed to the breaking of hydrogen bonds which cross-link the amide groups, forming a network.[15,16] The formation of this network is a slow process; therefore, these peaks do not appear in the thermograms of the annealed films because annealing was performed in the sample pan, immediately followed by rapid cooling (20 K/min) just before the measurement.

The glass steps $[\Delta c_p=0.1,\ldots,0.3$ J/(g K)] are relatively small, and the glass step of the cold-drawn film is broadened. The specific-heat step Δc_p decreases after annealing and particularly after cold drawing, but it increases again if the cold-drawn film is annealed. It seems that the amorphous phase changes from rigidity to more viscoelasticity.

The melting behavior (Fig. 2) is markedly affected by the preparation conditions. Cold drawing and particularly annealing after cold drawing lead to a much more pronounced endothermic heat-flow peak (melting peak) compared with the as-received film. In contrast, annealing of the as-received film leads to significant broadening and splitting of the melting peak. The area under the heat-flow peak is a measure of the enthalpy of fusion H_f

$$H_f=\frac{1}{mh}\int \Phi(T)dT$$

(m mass, h heating rate, and Φ heat flow). It is used to calculate the degree of crystallinity $c=H_f/H_{f,0}$, where $H_{f,0}$ is the enthalpy of fusion of 100% crystalline PA 11. A value $H_{f,0}=189$ J/g was used.[17] The results of these calculations are given in Table I. The cold-drawn and annealed films have the highest degree of crystallinity; however, the overall crystallinity is relatively low. Other authors give higher values of

TABLE I. Enthalpy of fusion H_f and degree of crystallinity c of BESHVO extruded film with different conditions of preparation.

	H_f (J/g)	c (%)
Melt quenched	49.4	26.1
Annealed	56.4	29.9
Cold drawn	61.4	32.5
Cold drawn, annealed	67.7	35.8

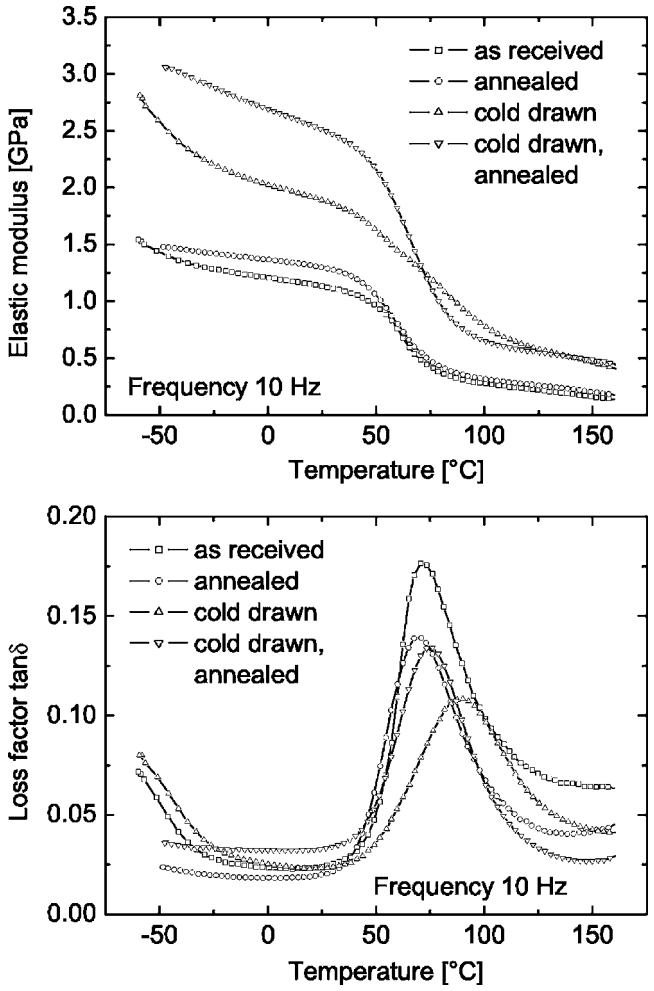

FIG. 3. Elastic modulus and mechanical loss factor of extruded PA-11 films after different preparations as indicated.

$H_{f,0}$ (222 J/g,[19] 244 J/g as a "rough estimate"[5]) which would result in even lower crystallinities. Furthermore, it can be concluded from the very different shapes of the melting peaks that the crystalline structure in the cold-drawn films is different from that of the as-received and then annealed films.

Several crystalline phases of PA 11 have been observed depending on preparation by different researchers.[20] Quenching from the melt yields no amorphous material, rather a short-range ordered smecticlike structure with randomly oriented hydrogen bonds and with a pseudohexagonal x-ray pattern which is called the δ' phase.[21] Annealing of the quenched PA 11 leads to transformation into the so-called α phase with a triclinic unit cell and a spherulithic film texture where the α phase constitutes the lamellae of the spherulithes. Growing of the α phase at the expense of the remaining amorphous regions leads to crystallites with very different perfection, because space and chain mobility become more and more limited with increasing crystallinity. This explains the appearance of a double-melting peak which is assumed to be caused by a superposition of melting and recrystallization processes. Cold drawing after melt quenching leads to formation of the ferroelectric phase where all hydrogen bonds are oriented perpendicular to the chains in the film plane. From our experimental experience this process works only well below the glass transition. Probably, crystallization within the α phase becomes very fast above the glass transition and happens already during heating before a ferroelectric phase can be formed by stretching at constant temperature. Because the stretched film was not heated before the DSC experiment, it can be assumed that its melting peak shows essentially the melting of the ferroelectric phase.

Annealing just below the melting after cold drawing leads to closer packing of the ferroelectric phase.[4,18] This finds its expression in an increase of the enthalpy of fusion.

B. Dynamic mechanical analysis (DMA)

The effects of cold drawing and annealing are shown in the temperature dependences of the elastic (Young's) modulus E' (the real part of the complex elastic modulus $E=E'+iE''$) and of the mechanical loss factor tan $\delta=E''/E'$ (Fig. 3). The step in E' and the corresponding peak of tan δ indicate the α relaxation which is connected with the glass transition. It is present in all films; however, it appears broader on the cold-drawn film, and its corresponding loss maximum is shifted to higher temperatures. Annealing of the as-received film enhances the modulus below T_g and reduces the loss factor. This can be explained with crystallization. Annealing of the cold-drawn film, in contrast, enhances the modulus below T_g significantly, but also recovers the glass step, enhances the corresponding loss-factor peak, and shifts it back to lower temperatures. This corresponds with the analogous behavior of the glass transition in DSC.

C. Dielectric relaxation spectroscopy (DRS)

DRS was performed in a wide frequency range in order to derive a relaxation map particularly of the glass-transition region. The temperature dependence of the permittivity and of the dissipation factor tan δ at 1.0 kHz for the first series of measurements is shown in Fig. 4. The second series gave analogous results (not shown here). The measurements confirm earlier results presented in Refs. 11 and 12. Here, we focus on the primary α relaxation. The secondary β process is only partly visible below 30 °C. Cold drawing increases the loss-factor intensity of the β process, while annealing has the opposite effect. On the melt-quenched film, the α peak is observed at about 65 °C. On the cold-drawn film, only a weak relaxation between 80 and 100 °C is visible as a shoulder. Annealing of the melt-quenched film only decreases the α peak, whereas annealing of the cold-drawn film seems to restore it. The increase of tan δ above 90 °C originates from free charges (dc conductivity and conductivity-current relaxation). It is significantly high-temperature shifted after cold drawing, but this effect is canceled by annealing.

D. Thermally stimulated depolariation currents (TSDCs)

TSDC measurements were performed in order to get additional information in the low-frequency range where the α peak is expected to appear at the glass-transition temperature. The TSDC method corresponds to measuring the dielectric losses at a very low equivalent frequency[22] (here

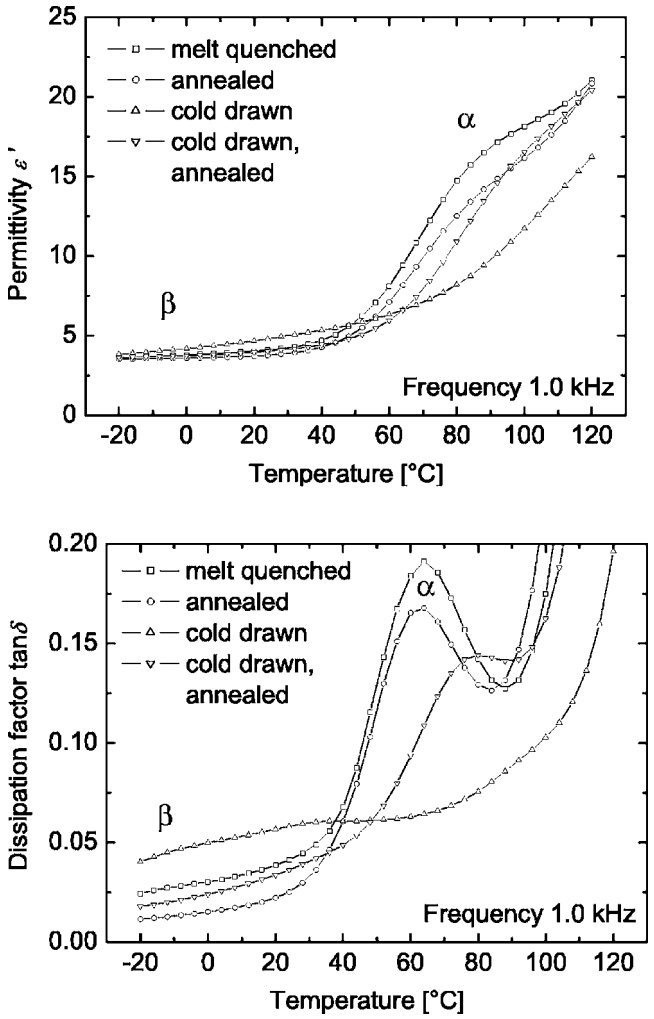

FIG. 4. Temperature dependence of the permittivity and the dielectric loss factor at 1 kHz on PA-11 films with different preparations as indicated (first series of measurement).

1–2 mHz). The normalised TSDC density $J_n = Id/(VA)$ (I current, d film thickness, V applied voltage, A electrode area) is plotted in Fig. 5 for the four differently prepared samples of the first series. The second-series measurements gave analogous results (not shown here). A broad asymmetric peak between −140 and −30 °C (low-temperature peak) and a strong peak with a peak temperature above 50 °C (high-temperature peak) are observed. The low-temperature peak is formed by the secondary β relaxation. This process was already discussed in Refs. 23 and 24. The α peak is expected at about 50 °C (glass transition). It is, however, not possible to observe it, because it is superimposed with the interfacial polarization, as will be seen in the next section. Because the interfacial-polarization peak is much more intense, it was not possible to obtain any information on the α peak, not even through measuring at several different polarization temperatures.

Cold drawing causes an intensity increase of the β process, but an intensity decrease and a high-temperature shift of the high-temperature peak which are also connected with a reduction of the conductivity. Annealing after quenching reduces the β intensity (probably due to loss of water) and slightly enhances the conductivity. Annealing after cold

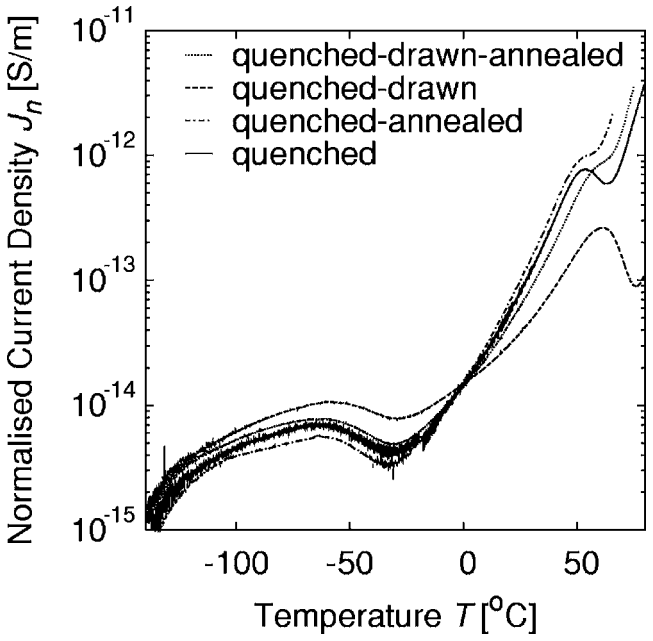

FIG. 5. Normalized TSDC on films of the first series with different preparations as indicated. The polarization was performed with $E_p = 1.0$ MV/m at $T_p = 60$ °C for $t_p = 5$ min.

drawing enhances the conductivity markedly but does not cause a peak shift. This underlines the fact that the TSDC high-temperature peak is an interface-polarization peak, not an α relaxation that is connected to the glass transition.

E. Detailed analysis of the dielectric data

The first series of measurements as presented in Fig. 4 and the second series of measurements were analyzed in more detail by fitting empirical relaxation functions to the data in order to obtain the temperature dependences of the loss-peak frequencies $f_{\max}$ of the relaxation processes that contribute to the dielectric spectrum (relaxation map) as well as their relaxation strengths $\Delta\epsilon$. Three relaxation processes (β_2, β_1, α) and an interface polarization must be considered along with the conductivity in order to obtain the best fit to the data.

The fits were performed at each temperature on the imaginary part ϵ'' of the dielectric function, using a function of the form

$$\epsilon''(f) = \Im\left\{\sum_{k=\mathrm{ccr},\alpha,\beta_1,\beta_2} \frac{\Delta\epsilon_k}{[1+(if/f_{c,k})^{m_k}]^{n_k/m_k}}\right\} + \frac{\sigma_{\mathrm{dc}}}{2\pi f \epsilon_0}. \quad (1)$$

The indices stand for the different relaxation mechanisms (α, β_1, β_2) and for the conductivity-current relaxation (ccr). The ccr refers to accumulation of charges at the end of conducting paths under conditions of dc conductivity (interface polarization). The last term of Eq. (1) describes the conductivity, with a dc value σ_{dc} and a slope of −1 in the log-log plot of ϵ'' versus frequency; ϵ_0 is the vacuum permittivity. The term in the sum represents a Havriliak-Negami function,[25] with $\Delta\epsilon$ the dielectric strength, and m and n the slopes of the peak for low ($f < f_c$) and high frequencies ($f > f_c$), respectively. The characteristic frequency f_c is connected to the peak frequency $f_{\max}$ through the relation:

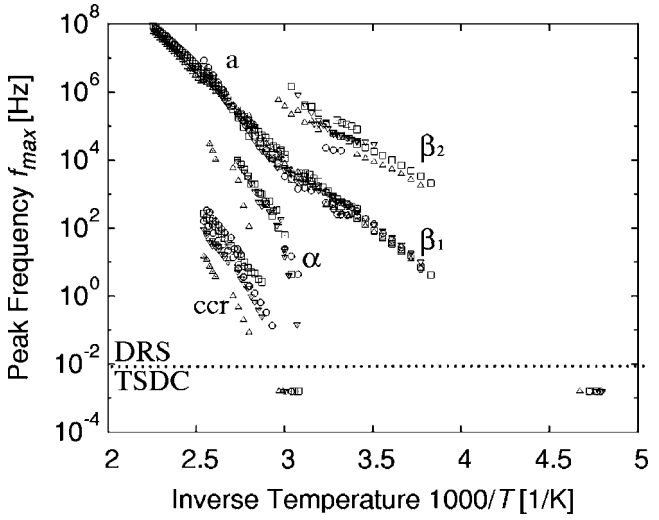

FIG. 6. Arrhenius plot (relaxation map) of the peak frequencies $f_{\max}$ determined from the fit to the experimentally observed dielectric spectrum (DRS) and of the equivalent frequencies f_{eq} calculated from the corresponding TSDC curves vs the inverse temperature $1000/T$ (second series: □ melt quenched, ○ melt quenched and annealed, △ melt quenched and cold drawn, ▽ melt quenched, cold drawn, and annealed; first series: same symbols with a dot).

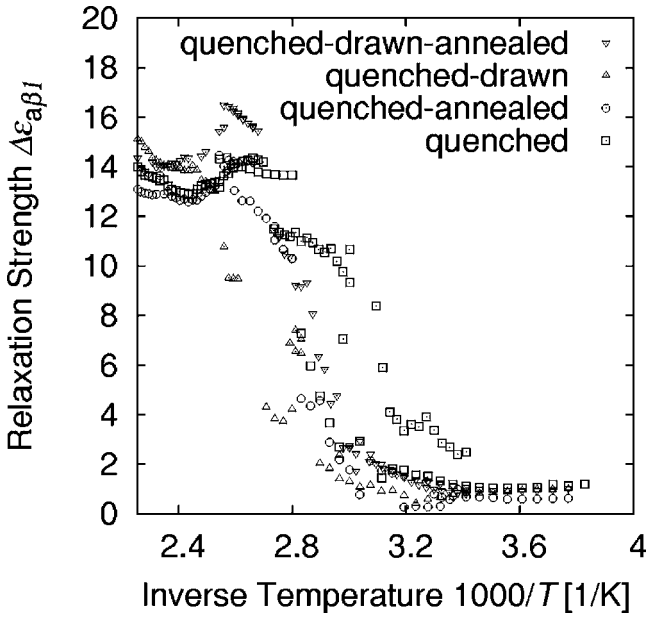

FIG. 7. Relaxation strength $\Delta\epsilon$ of the $\mathbf{a}\beta_1$ relaxation from the HN fit to the experimentally observed dielectric spectrum for various structures as indicated in the legend (symbols like in Fig. 6).

$$f_{\max} = f_c \left(\frac{\sin m\pi/(2+2n/m)}{\sin n\pi/(2+2n/m)} \right)^{1/m}. \tag{2}$$

Unlike the asymetric α mechanism, the β_1, β_2 relaxations and the interfacial polarization were found to be symmetric, as expected for such processes. Consequently, the number of parameters was reduced by setting $m=n$ in these cases. In other words, the Cole-Cole instead of the Havriliak-Negami model is used.

Figure 6 presents the Arrhenius plot for all samples (both series of measurements). Along with the results of the fitting for $f_{\max}$, the data resulting from the TSDC measurements (points in the millihertz range) are also shown. Moving from the low-temperature high-frequency end to the opposite, one observes the β_2, β_1, α, and ccr traces, as marked on the plot. The relaxation map agrees well with a scenario that was suggested by Donth.[26] According to this scheme, the β_1 trace is the low-temperature part of the so-called $\mathbf{a}\beta_1$ trace that consists of three different regions: the high-temperature process (**a** or Williams-Götze process) below $1000/T=2.6$, the crossover region (C region) where the α process sets in and runs parallel to the **a** process, and the low-temperature region ($1000/T>3.0$) where the α process becomes significantly curved and where the separate β relaxation (Johari-Goldstein process, here β_1) is observed. There is a bend in the $\mathbf{a}\beta_1$ trace at about $1000/T=3$ that probably marks the temperature at which the **a** process vanishes, while the β_1 process begins.

There is very good agreement of the extrapolated β_1 and β_2 (not shown) traces with the TSDC data. The β_1 process shows Arrhenius behavior. Fitting the data of the β_1 trace with the Arrhenius equation

$$f_{\max} = f_0 \exp\left(-\frac{E_a}{kT} \right), \tag{3}$$

where k is Boltzmann's constant, yields the activation energy E_a and the preexponential factor f_0 of the β_1 process. The TSDC data were also taken into consideration. Values of 0.71–0.80 eV and 3.1×10^{14} to 1.1×10^{16} Hz are obtained. The $\mathbf{a}\beta_1$ and the β_2 traces show no significant dependence on various structural features that are formed by annealing and stretching.

Due to the overlap of the peaks in the region where the α process is also present, fitting was not always possible. In particular, the determination of the parameters of the α relaxation was hindered, since it lies directly between the stronger β_1 and interfacial-polarization processes. Thus, only a few data points were acquired for the processes in this important region and their scatter is significant. From the acquired data, one can see that the α process as well as the interfacial polarization have non-Arrhenius behavior. Due to the small number of data points, Vogel-Fulcher-Tammann (VFT) fits for the α process would carry a significant uncertainty. Nevertheless, the extrapolation of their traces to low frequencies seems to coincide with the TSDC data for the high-temperature peak. Given the much higher intensity of the interfacial polarization, this explains the fact that the α relaxation cannot be observed with the TSDC technique. In the crossover region (about $2.6<1000/T<3.0$), the α trace appears about one frequency decade below the **a** trace, before bending into VFT behavior towards the glass transition.

Figures 7 and 8 show the temperature dependences of the relaxation strength $\Delta\epsilon$ of the $\mathbf{a}\beta_1$ and α processes, respectively. Below the glass transition ($1000/T_g\approx3$), β_1 has a very low strength $\Delta\epsilon_{\beta_1}\approx1$, which is almost independent on temperature. At the glass transition, α appears with $\Delta\epsilon_\alpha$ having a high value ranging from 3 to 10 for the different

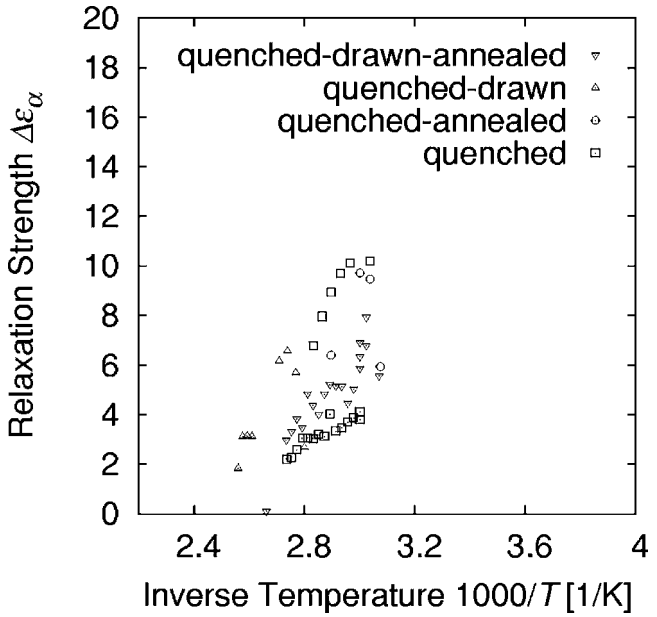

FIG. 8. Relaxation strength $\Delta\epsilon$ of the α relaxation from the HN fit to the experimentally observed dielectric spectrum for various structures as indicated in the legend (symbols like in Fig. 6).

samples. With increasing temperature (up to the α onset), $\Delta\epsilon_\alpha$ decreases, while $\Delta\epsilon_{\beta_1}$ increases accordingly. From an extrapolation of the $\Delta\epsilon_\alpha$ data, it is expected that the α process vanishes at about $1000/T=2.5$ ($T=127$ °C) which defines the α onset. The sum $\Delta\epsilon_\alpha+\Delta\epsilon_{\mathbf{a}\beta_1}=14\pm3$ remains constant in this temperature range, indicating that the nature of the relaxing units is the same for all processes. From a look at the chemical structure, it is concluded that the relaxing units are formed essentially by the amide-group dipoles. Below T_g, only the β relaxation is possible. Its strength is low, because only few units can relax in the "islands of mobility."[26] Above T_g, the α process allows the remaining units to relax. The strength of $\mathbf{a}\beta_1$ increases, even though the relaxation time of most dipoles just above T_g is determined by the much slower α relaxation. As the temperature increases, more and more dipoles find themselves in regions of higher mobility and relax following the faster **a** process until α finally dies out. At still higher temperatures, only the **a** process remains, with a constant dielectric strength.

In Fig. 6 the α relaxation and also the interface polarization of the cold-drawn films are confirmed to be high-temperature shifted (slowed down), but this shift is at least partially removed after annealing. Accordingly, the increase of $\Delta\epsilon$ for the $\mathbf{a}\beta_1$ process with increasing temperature (the transition from β_1 to **a**, Fig. 7) is considerably high-temperature shifted on the cold-drawn samples, while annealing after cold drawing reduces this shift at least partially.

IV. SUMMARY AND CONCLUSIONS

Under the assumption of a two-phase morphology, there is clearly something missing between the small glass steps and the relatively low overall crystallinity of all four structures. These experimental results suggest that there exists a fraction of the material that forms a rigid amorphous phase (RAP). Rigidity may originate from pinning polymer chains on crystallites but also by cross-linking via hydrogen bonds. It is particularly dominant in the cold-drawn film, thus cold drawing not only enhances the crystallinity but also the rigidity of the amorphous phase. However, a RAP is also present in the quenched film, indicating that it is practically impossible to obtain a viscoelastic amorphous phase by rapid cooling.

The temperature dependences of the elastic modulus (Fig. 3) and the dielectric permittivity (Fig. 4) show analogous results, though extruded films were used for DMA and melt-quenched ones for DRS. In particular, the α relaxation that is connected with the glass transition is weakened and slowed down by cold drawing but at least partly recovered by subsequent annealing. Furthermore, the glass transitions found in DSC (Fig. 1) correspond with the dielectric results presented in Fig. 6 where the α traces bend around $1000/T=3.0$ (60 °C) at 10^{-2} Hz which marks the glass transition.[26] In addition, the dielectric results which were analyzed in more detail show that there is no fundamental difference between all four structures regarding the amorphous regions: A glass transition and a corresponding α relaxation were always found. The dielectric relaxations obey a time-temperature scenario that is known from glass-forming liquids but was also found on polymers.[26] Consequently, there exists always some molecular mobility in the amorphous phase above the glass transition, even in the cold-drawn film. The observed slowing down and decrease of the α peak after cold drawing can be understood as a consequence of increased rigidity in the amorphous phase. Motion of charge carriers is only possible when facilitated by chain motion. Therefore, the interface polarization is also slowed down by cold drawing.

Annealing just below the melting region after cold drawing has two different effects. First, it leads to recrystallization in a morphology different from the one found after annealing of a nonstretched film. This is suggested by the very different shapes of the DSC melting peaks of the two annealed films. By means of wide-angle x-ray diffraction (WAXD), Lee *et al.*[4] and later Takahashi *et al.*[18] found a significant decrease in spacing between hydrogen-bonded sheets after annealing that makes field-induced rotation of amidegroups within ferroelectric domains impossible. Thus, with annealing of a cold-drawn film one ends up in a crystalline structure that cannot be poled because the orientations of amide-group dipoles are locked. Second, it removes ordered structures within the amorphous phase where the polymer chains had been aligned more or less in parallel, but did not form a ferroelectric domain. By means of WAXD, Jolly *et al.*[27] showed that uniaxial extension of PA 11 induces a preferred orientation of macromolecules also in the amorphous phase. In other words, annealing after cold drawing causes the rigid amorphous phase to relax ending up in a stronger phase separation between the crystalline phase and a more viscoelastic amorphous phase. This process leads to a recovery of the glass step and the dielectric and mechanical α relaxation that is connected with the glass transition.

ACKNOWLEDGMENTS

The authors gratefully acknowledge financial support from TOTAL S. A., F-92400 Courbevoie, France, project DS 2134, and from the IKYDA program [Greek State Scholarships Foundation (IKY), Deutscher Akadamischer Austauschdienst (DAAD)]. The PA 11 was kindly provided by Arkema Research and Development Centre, F-27470 Serquigny, France. The authors are indebted to Dirk Heinrich (University of Potsdam) for designing the hot press, to Monika Ehlert (University of Potsdam) for performing the DSC measurements, and to Dr. Wolfgang Stark (Federal Institute for Materials Research and Testing, Berlin, Germany) for support during the DMA measurements.

[1] J. I. Scheinbeim and B. A. Newman, Trends Polym. Sci. **1**, 394 (1993).
[2] R. G. Kepler and R. A. Anderson, Adv. Phys. **41**, 1 (1992).
[3] Y. Takase, J. W. Lee, J. I. Scheinbeim, and B. A. Newman, Macromolecules **24**, 6644 (1991).
[4] J. W. Lee, Y. Takase, B. A. Newman, and J. I. Scheinbeim, J. Polym. Sci., Part B: Polym. Phys. **29**, 279 (1991).
[5] A. Xenopoulos and B. Wunderlich, J. Polym. Sci., Part B: Polym. Phys. **28**, 2271 (1990).
[6] C. Alvarez, I. Šics, A. Nogales, Z. Denchev, S. S. Funari, and T. A. Ezquerra, Polymer **45**, 3953 (2004).
[7] B. Wunderlich, Prog. Polym. Sci. **28**, 383 (2003).
[8] G. Strobl, Prog. Polym. Sci. **31**, 398 (2006).
[9] A. Nogales, T. A. Ezquerra, F. Batallán, B. Frick, E. López-Cabarcos, and F. J. Baltá-Calleja, Macromolecules **32**, 2301 (1999).
[10] R. J. Seyler, J. Atmos. Terr. Phys. **49**, 491 (1997).
[11] P. Frübing, A. Kremmer, J. Ganster, P. Pissis, and R. Gerhard-Multhaupt, *Proceedings of the 11th International Symposium on Electrets* (IEEE, Piscataway, NJ, 2002), p. 88.
[12] P. Frübing, A. Kremmer, W. Neumann, R. Gerhard-Multhaupt, and I. L. Guy, IEEE Trans. Dielectr. Electr. Insul. **11**, 271 (2004).
[13] C. Schick, in *Temperature Modulated Differential Scanning Calorimetry (TMDSC): Basics and Applications to Polymers*, Handbook ot Thermal Analysis and Calorimetry, Vol. 3, edited by Z. D. Cheng (Elsevier, Amsterdam, 2002) p. 724.
[14] H. E. Bair, in *Glass Transition Measurement by DSC*, Assignment of the Glass Transition, ASTM STP 1249, edited by R. J. Seyler (American Society for Testing and Materials, Philadelphia, 1994), p. 57.
[15] G. A. Gordon, J. Polym. Sci., Part A-2 **9**, 1693 (1971).
[16] L. Ibos, C. Maraval, A. Bernès, G. Teyssèdre, C. Lacabanne, S.-L. Wu, and J. I. Scheinbeim, J. Polym. Sci., Part B: Polym. Phys. **37**, 715 (1999).
[17] Q. Zhang, Z. Mo, S. Liu, and H. Zhang, Macromolecules **33**, 5999 (2000).
[18] Y. Takahashi, M. Shimomura, M. Kutani, and T. Furukawa, Polym. J. (Tokyo, Jpn.) **29**, 234 (1997).
[19] R. Greco and L. Nicolais, Polymer **17**, 1049 (1976).
[20] H. S. Nalwa, *Ferroelectric Nylons*, in Ferroelectric polymers, edited by H. S. Nalwa (Dekker, New York, 1995) p. 286.
[21] L. J. Mathias, D. G. Powell, J. P. Autran, and R. S. Porter, Macromolecules **23**, 963 (1990).
[22] J. van Turnhout, *Thermally Stimulated Discharge in Polymer Electrets* (Elsevier, Amsterdam, 1975).
[23] R. M. Neagu, E. Neagu, A. Kyritsis, and P. Pissis, J. Phys. D **33**, 1921 (2000).
[24] L. Ibos, A. Bernès, G. Teyssèdre, C. Lacabanne, S.-L. Wu, and J. I. Scheinbeim, *Proceedings of the Tenth International Symposium on Electrets* (IEEE, Piscataway, NJ, 1999), p. 623.
[25] S. Havriliak and S. Negami, J. Polym. Sci., Part C: Polym. Symp. **14**, 99 (1966).
[26] E. Donth, *The Glass Transition* (Springer, Berlin, 2001), Chaps. 2.2.1 and 2.5.3, p. IX.
[27] L. Jolly, A. Tidu, J.-J. Heizmann, and B. Bolle, Polymer **43**, 6839 (2002).